Structural Basis for Vapoluminescent Organoplatinum Materials Derived from Noncovalent Interactions as Recognition Components

Wei Lu,[a] Michael C. W. Chan,[a] Nianyong Zhu,[a] Chi-Ming Che,*[a] Zhike He,[b] and Kwok-Yin Wong*[b]

Abstract: The spectroscopic properties and crystal structures of a series of platinum(II) complexes bearing functionalized σ-alkynyl groups, namely $[(t\mathrm{Bu_2bpy})\mathrm{Pt}(\mathrm{C{\equiv}CAr})_2]$ ($t\mathrm{Bu_2bpy}$ = 4,4′-bis-*tert*-butyl-2,2′-bipyridine, Ar = 4-pyridyl, **1**; 3-pyridyl, **2**; 2-pyridyl, **3**; 4-ethynylpyridyl, **4**; 2-thienyl, **5**; pentafluorophenyl, **6**) have been studied. Solid-state emissions of **1** and **6** are dependent on their crystallinity. Reversible and selective vapoluminescence was observed for **1** and **6** in the presence of chlorocarbon vapors. For solid **1**, dramatic enhancement of green luminescence is observed upon sorption of CH_2Cl_2 or $CHCl_3$ vapor. The excimeric orange emission for solid **6** is switched to monomeric green emission upon exposure to CH_2Cl_2 vapor. The luminescent responses of a thin film of **1** towards various organic vapors have also been examined. In the crystallographically determined structure of **1**·CH_2Cl_2, the bis(acetylide) moiety acts as the receptor berth for a CH_2Cl_2 molecule through concerted C–H···π(C≡C) interactions, while Cl···Cl interactions connect the CH_2Cl_2 molecules into infinite linear chains. The observed crystal lattices are arranged into scaffolds of varying porosity by weak C–H···N(py) (**1**·CH_2Cl_2, **1**·CH_3CN, **4**·DMF) and C–H···F–C (**6**, **6**·CH_3CN) interactions. The correlation between the crystal structures of **1**·CH_2Cl_2, **1**·CH_3CN, **2**, **4**·DMF, **5**, **6**, and **6**·CH_3CN and their vapoluminescence suggests that weak nonconventional hydrogen-bonding interactions preside over the reversible sensing and signalling processes.

Keywords: alkyne ligands · inclusion compounds · noncovalent interactions · platinum · vapoluminescence

Introduction

Weak noncovalent interactions are fundamental to the design, operation, and efficiency of molecular sensors and switches. The dynamic nature of these contacts and their fragility allow rapid association–dissociation between host and guest under ambient conditions. This feature is critical to achieve sensitivity and specificity in the detection of molecular species. Weak C–H···π(C≡C) interactions in the solid state between molecules containing acidic C–H groups and metal–acetylide or –alkyne compounds are well known in the literature.[1] In particular, Mingos and co-workers identified such contacts in chloroform solvates of binuclear gold(I) ethynediyl complexes. Although they emphasized their significance with regards to molecular recognition, applications have yet to be realized.[1a]

Luminescent probes constitute a convenient and diverse class of sensory devices with practical applications.[2] Conventional photoluminescent sensors yield varying emission intensities in response to changes in analyte concentration under constant light irradiation. Ideally, recognition of analyte(s) and the corresponding response should be selective and reversible. Transition-metal complexes have been extensively studied as luminescent sensory materials for O_2, mo-

[a] Prof. Dr. C.-M. Che, W. Lu, Dr. M. C. W. Chan, Dr. N. Zhu
Department of Chemistry and Open Laboratory of Chemical Biology of the Institute of Molecular Technology for Drug Discovery and Synthesis
The University of Hong Kong, Pokfulam Road
Hong Kong SAR (China)
Fax: (+852) 2857-1586
E-mail: cmche@hku.hk

[b] Prof. Dr. K.-Y. Wong, Dr. Z. He
Department of Applied Biology and Chemical Technology and Central Laboratory of the Institute of Molecular Technology for Drug Discovery and Synthesis
The Hong Kong Polytechnic University, Hunghom, Kowloon
Hong Kong SAR (China)
Fax: (+852) 2364-9932
E-mail: bckywong@polyu.edu.hk

Supporting information for this article is available on the WWW under http://www.chemeurj.org/ or from the authors. Absorption spectra of **1** in various solvents at 298 K; solid-state emission spectra of **1** with different crystallinity at 77 K; fluid and solid-state emission spectra of **2**–**5**; emission and excitation spectra of various crystalline forms of **6**; diagram showing set-up for determining the emission response of the sensing film towards VOCs; relative emission intensity versus vapor concentration of CH_2Cl_2 and $CHCl_3$ for the film prepared with **1**; additional crystallographic plots.

 DOI: 10.1002/chem.200305322

lecular ions and changes in pH.[3] Recent reports have described complexes that exhibit vapochromic behavior and give dramatic photophysical changes in the presence of volatile organic compounds (VOCs) and gases.[4–10] These luminescent probes can be divided into three main types in view of the nature of the host–guest interaction mechanism: a) discrete metallocyclophanes possessing large cavities that can accommodate VOC molecules;[5] b) oxygen-quenching phosphorescent lumophores tailored into mesoporous materials such as zeolites, rubbers, and sol–gels;[6] c) molecular solids that alter their crystal lattice or chemical structures upon sorption of vapors. Examples of category c) include $[Au_3(CH_3N{=}COCH_3)_3]$,[7] $[Au(S_2CN(C_5H_{11})_2)]_2$,[8] $[PtL_4][M(CN)_4]$ (L = arylisonitrile; M = Pt, Pd),[9] and $[CuI(4\text{-methylpyridine})]_n$ ($n = 4$ and ∞).[10] Mann and co-workers have performed extensive studies on the $[PtL_4][M(CN)_4]$ (M = Pt, Pd) double salts. They concluded that the vapochromic behavior is induced by crystal-lattice disruptions affecting the Pt···Pt/Pd interactions, and hence the emissive excited state.[9] Perturbation of metal–metal excited states have also been invoked to rationalize the VOC-detecting abilities of the gold(I) dimeric and trimeric luminescent complexes.[7,8]

Many investigations have shown that the color and emissive properties of crystalline α-diimine and/or cyclometalated platinum(II) solids are highly dependent upon the chosen anion and solvent(s) for the precipitation/recrystallization. Differences in the extent of π–π and/or Pt···Pt interactions are usually cited to rationalize these phenomena.[11] Indeed, the spectroscopic and excited-state properties of luminescent platinum(II) materials are often sensitive to solid-state effects. The sensitivity of the photoluminescence of coordinatively unsaturated platinum(II) complexes to their microenvironment alludes to their potential role as practical molecular sensors.[12] Conceptually, "switch-on" vapoluminescent sensors that provide a positive luminescent response are advantageous because greater sensitivity (contrast in signaling against dark background) and selectivity becomes possible.[13] We now describe neutral organoplatinum solids containing functionalized arylacetylide ligands that undergo dramatic luminescent responses upon exposure to selected VOCs. We conceived that the (weak) binding capabilities of functionalized arylacetylide moieties would represent potential recognition elements. Importantly, a number of crystal structures, both solvated and unsolvated, have been determined. This collection of structural data provides the foundation from which, by scrutiny and comparison of weak intermolecular forces in the crystal lattices, elucidation of the factors and/or mechanisms leading to vapoluminescence and selectivity become possible. This work, to the best of our knowledge, represents the first example of a chemosensing material derived from weak noncovalent recognition by metal–acetylide moieties, and highlights the possible role of conjugated alkynyl units as relay components in luminescent metallosensors.

Results

A series of platinum(II) σ-alkynyl complexes (**1–6**, Scheme 1) supported by the tBu$_2$bpy (4,4′-bis-*tert*-butyl-2,2′-bipyridine) ligand was prepared by treating the $[(t\text{Bu}_2\text{-bpy})PtCl_2]$ precursor with the corresponding arylacetylene substrate according to Sonogashira's method (CH_2Cl_2/iPr$_2$NH/CuI). All derivatives are air- and photo-stable crystalline solids with good solubility, particularly in CH_2Cl_2 and $CHCl_3$. In the literature, two methods to generate platinum(II) bis(acetylide) complexes containing α-diimine ligands are reported, namely, the aforementioned Sonogashira protocol[14,15b–d] and ligand substitution between $[(cod)Pt(C{\equiv}CR)_2]$ (cod = 1,5-cyclooctadiene) and α-diimine.[15a,d] The latter was employed to synthesize $[(phen)Pt(C{\equiv}CPh)_2]$ (phen = 1,10-phenanthroline), the first luminescent member of this family to be reported.[15a] All attempts in the present study to prepare 4,4′-dimethyl-2,2′-bipyridine and substituted 1,10-phenanthroline analogues bearing 4-pyridylacetylide auxiliaries afforded intractable powders that are insoluble in common organic solvents.

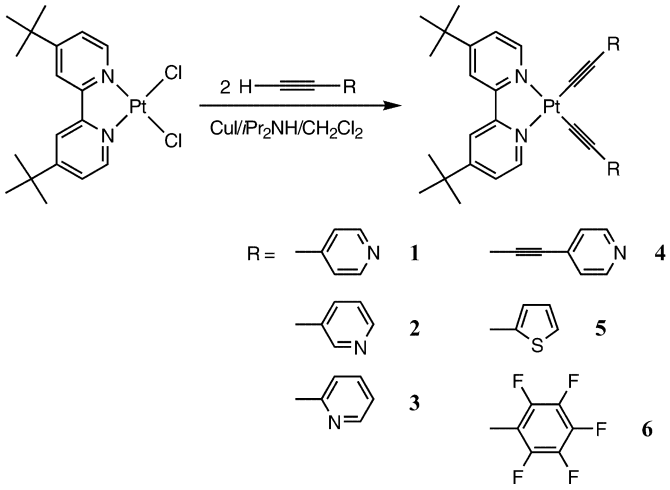

Scheme 1.

Spectroscopic properties: The UV/Vis absorption spectra of **1–6** in CH_2Cl_2 at 298 K are depicted in Figure 1. In these spectra, two transition bands in the 250–320 ($\varepsilon \approx 4 \times 10^4$ dm^3 mol^{-1} cm^{-1}) and 350–470 nm ($\varepsilon \approx 1 \times 10^4$ dm^3 mol^{-1} cm^{-1}) ranges are prominent. The absorption maximum of the low-energy band is dependent on the electronic affinity of the

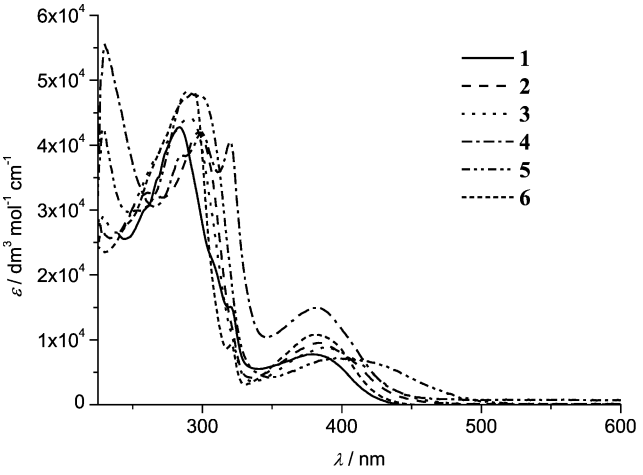

Figure 1. UV/Vis absorption spectra of **1–6** in CH_2Cl_2 at 298 K.

acetylide substituents. Namely, complex **5**, bearing electron-donating 2-thienyl groups, displays an absorption maximum at 410 nm, while this band is blue-shifted to $\lambda_{max} = 381$ nm for **6** with pentafluorophenyl moieties. The energy of the low-energy band also varies according to solvent polarity. For example, this absorption band for **1** exhibits a blue shift from $\lambda_{max} = 410$ to 378 and 372 nm when the solvent polarity increases from toluene to CH_2Cl_2 and ethanol respectively (see Supporting Information).

The solution and glassy emission data of complexes **1–6** are summarized in Table 1. All complexes are strongly emissive in fluid solutions and alcoholic glasses with lifetimes in the microsecond regime. The emission energies of these complexes are dependent upon solvent polarity, following the same trend as that detected in the absorption spectra. For example, the emission maximum of **1** exhibits a blue shift from 519 to 510 and 501 nm when the solvent polarity increases from toluene to CH_2Cl_2 and ethanol, respectively.

Table 1. Emission data of **1–6** in various media (concentration $\sim 1\times10^{-5}$ mol dm^{-3}).

Complex	λ_{max} [nm] (τ [μs]; ϕ)			
	EtOH (298 K)	CH_2Cl_2 (298 K)	toluene (298 K)	MeOH/EtOH 1:5 (77 K)
1	501 ($\leq$0.1; 0.021)	510 (0.14; 0.08)	519 (0.61; 0.64)	456, 483 (3.9)
2	532 ($\leq$0.1; 0.065)	531 (0.81; 0.66)	540 (1.5; 0.54)	456, 480 (3.9)
3	501 ($\leq$0.1; 0.043)	520 (0.38; 0.32)	526 (1.2; 0.51)	454, 484 (3.8)
4	495, 510 (sh) ($\leq$0.1; 0.096)	498, 515 (sh) (0.51; 0.31)	516, 540 (sh) (1.1; 0.19)	487, ~520, 545, 618 (28)
5	~595 ($\leq$0.1; 0.008)	592 (0.17; 0.03)	598 ($\leq$0.1; 0.021)	503, 537 (17)
6	500 ($\leq$0.1; 0.017)	501 (0.17; 0.05)	512 (0.27; 0.70)	450, 479 (4.9)

Interestingly, the solid-state emission of **1** is highly dependent on its crystallinity and recrystallization medium (Figure 2). When a CH_2Cl_2/Et_2O mixture was used for recrystallization, bright green-yellow crystals of **1**·CH_2Cl_2 were obtained. At 298 K, crystalline **1**·CH_2Cl_2 displays an intense emission at λ_{max} 517 nm with vibronic progression of about 1300 cm^{-1} (Figure 2b). This emission is virtually identical in energy to that recorded in CH_2Cl_2. Yellow crystals of **1**·CH_3CN, obtained by recrystallization in CH_3CN, exhibit a broad emission at $\lambda_{max} = 560$ nm, which is slightly red-shifted from **1**·CH_2Cl_2 but with similar vibronic progressions (Figure 2c). To the naked eye, a crystalline sample of **1**·CH_2Cl_2 emits noticeably more intensely than **1**·CH_3CN under comparable conditions. Interestingly, the emission intensity for a fine powder of **1**, obtained by grinding the crystalline samples, is extremely low; the vibronic emission in the 480–600 nm range is effectively quenched and a very weak structureless broad band centered at 640 nm is detected (Figure 2d). Upon further investigation, we observed that when the dull brown-yellow powder of **1** is exposed to CH_2Cl_2 or $CHCl_3$ vapor, an intense green emission is produced under UV irradiation. When this powder is subsequently subjected to heat or reduced pressure, the emission vanishes and the powder reverts to its original dull color. At 77 K, the emission energies and spectral shapes of these crystal forms are similar to those recorded at 298 K, but the emission intensities become comparable (see Supporting Information).

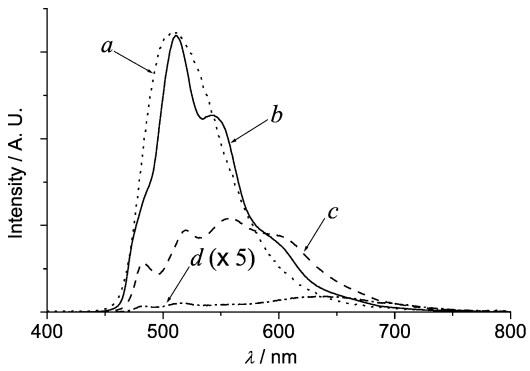

Figure 2. Emission spectra (λ_{ex}=350 nm) of **1** in CH_2Cl_2 solution (*a*) and in solid state at 298 K with different crystallinity (*b*: **1**·CH_2Cl_2 crystals; *c*: **1**·CH_3CN crystals; *d*: powder form obtained by grinding **1**·CH_2Cl_2 crystals; *a* and *b* are normalized to facilitate comparison).

The solid-state emission spectra of **2–5** at both 298 and 77 K have also been recorded (see Supporting Information for spectra). For **2** and **5**, the solid-state emissions at 298 and 77 K are structured and comparable in energy to that recorded in CH_2Cl_2 solution. The solid-state emission spectra of **3** at 298 K and **4** at 77 K both exhibit two emission bands. The high-energy band is structured (vibronic progression approximately 1300 cm^{-1}) and similar to their CH_2Cl_2 emission, while the low-energy band (λ_{max}=618 nm for both **3** and **4**) is structureless. Importantly, the energies and intensities of the solid-state emissions of **2–5** are unaffected by the presence of VOCs.

The solid-state emission of **6** is also dependent on its crystallinity and recrystallization medium (Figure 3). Recrystallization from a CH_2Cl_2/Et_2O mixture afforded a bright green-yellow crystalline form that displays an intense, poorly resolved emission at $\lambda_{max} = 500$ nm at 298 K (Figure 3b); this emission is virtually identical in energy to that recorded in CH_2Cl_2. The corresponding excitation spectrum monitored at $\lambda_{em} = 500$ nm for this crystalline form shows absorption cut-off at around 460 nm (see Supporting Information). Similarly, green-yellow crystals of **6**·CH_3CN, obtained from a saturated CH_3CN solution, exhibits an intense emission at λ_{max}=503 nm (Figure 3c), which is similar to that recorded for the solid recrystallized from a CH_2Cl_2/

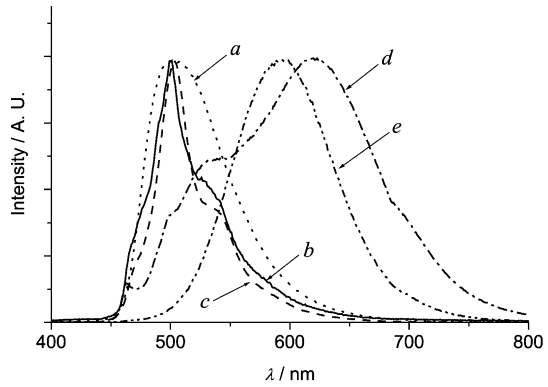

Figure 3. Normalized emission spectra ($\lambda_{ex}=350$ nm) of **6** in CH_2Cl_2 solution (*a*) and in solid state at 298 K with different crystallinity [*b*: green form from CH_2Cl_2/Et_2O; *c*: crystals of **6**·CH_3CN; *d*: powder form obtained by grinding **6**·CH_3CN crystals; *e*: orange form obtained from benzene].

Et_2O mixture. On the other hand, a fine powder of **6**, obtained by grinding the crystalline green-yellow samples, is highly luminescent at 298 K with a structured emission in the 463–545 nm range and an intense, structureless emission at λ_{max} = 620 nm (Figure 3d). Orange crystals of **6**, grown from a cooled benzene solution, exhibit an intense, structureless emission at λ_{max} 595 nm (Figure 3e) that is noticeably red-shifted compared to the green-yellow form of **6**. The excitation spectrum for the orange form (monitored at λ_{em} 595 nm) exhibits low-energy cut off at 463 nm, which resembles that observed for the green-yellow crystals obtained from CH_2Cl_2/Et_2O. When the orange form of **6** is exposed to CH_2Cl_2 vapor, the orange emission is gradually replaced by green emission ($\lambda_{em} \approx 500$ nm) under UV irradiation, but when this sample is subjected to reduced pressure, the intense orange emission is restored.

Crystal structures and weak noncovalent interactions: The X-ray structures of **1**·CH_2Cl_2 (grown from CH_2Cl_2/Et_2O), **1**·CH_3CN (CH_3CN), **2** (CH_2Cl_2/Et_2O), **4**·DMF (DMF/Et_2O), **5** (CH_2Cl_2/Et_2O), **6** (benzene) and **6**·CH_3CN (CH_3CN) have been determined (Table 2).

For **1**·CH_2Cl_2 (Figure 4, top), a molecular structure with C_{2v} symmetry is found, with the bpy and 4-pyridyl ring systems coplanar, and the CH_2Cl_2 molecule located below this plane. The H17–C1 and H17–C2 distances are 2.81 and 2.85 Å respectively, which are slightly shorter than the combined van der Waals radii for H and C (2.9 Å),[16] and can be compared to the C–H···π(C≡C) distances in $(Ar_3P)AuC{\equiv}CAu(PAr_3)\cdot(CHCl_3)_n$ ($n=2$, $Ar_3=NpPh_2$; $n=6$, $Ar_3=Np_2Ph$; Np = naphthyl) (d_{H-C} 2.45–2.70 Å),[1a] [(η^5-C_5H_5)W(C≡CC_3H_5)(PMe_3)$(CO)_2$]·CH_2Cl_2 (d_{H-C} 2.45 and 2.58 Å)[1b] and $(CH_3)_3Si{-}C{\equiv}C{-}C{\equiv}C{-}Si(OCH_2CH_2)_3N\cdot(CHCl_3)_2$ (d_{H-C} 2.54(3)-2.82(3) Å).[17] The C17-H17-C1 and C17-H17-C2 angles are 129 and 143°, respectively. We propose that weak C–H···π(C≡C) interactions exist between the two acidic protons of the CH_2Cl_2 molecule and the bis(acetylide) moiety. Furthermore, these solvent molecules are arranged through weak Cl···Cl contacts[18,19a] ($d_{Cl-Cl}=3.43$ Å, $\theta_{C17\text{-}Cl1\text{-}Cl2}=173°$, $\theta_{Cl1\text{-}Cl2\text{-}C17}=121°$) into infinite $(CH_2Cl_2)_\infty$ chains. These are accommodated within hydrophobic channels (with van der Waals diameters of approximately 6.0 Å) running along the *c* axis of the crystal lattice (Figure 4, middle and bottom). This network of weak noncovalent interactions is completed by C–H···N hydrogen bonding interactions[19] ($d_{H-N}=2.71$ Å, $\theta_{C\text{-}H\text{-}N}=173°$) be-

Table 2. Crystal data.

	1·CH_2Cl_2	**1**·CH_3CN	**2**	**4**·DMF	**5**	**6**	**6**·CH_3CN
formula	$C_{33}H_{34}Cl_2N_4Pt$	$C_{34}H_{35}N_5Pt$	$C_{32}H_{32}N_4Pt$	$C_{39}H_{39}N_5OPt$	$C_{30}H_{30}N_2PtS_2$	$C_{34}H_{24}F_{10}N_2Pt$	$C_{36}H_{27}F_{10}N_3Pt$
F_w	752.65	708.77	667.71	788.84	677.77	845.64	886.70
color	greenish yellow	yellow	yellow	yellow	orange	orange yellow	greenish yellow
T [K]	301	301	301	301	301	293	293
crystal size [mm^3]	0.40×0.10×0.07	0.25×0.15×0.10	0.4×0.2×0.1	0.25×0.2×0.1	0.35×0.2×0.15	0.3×0.2×0.08	0.4×0.15×0.05
crystal system	orthorhombic	triclinic	monoclinic	triclinic	triclinic	triclinic	triclinic
space group	*Pnma*	$P\bar{1}$	$P2_1/n$	$P\bar{1}$	$P\bar{1}$	$P\bar{1}$	$P\bar{1}$
a [Å]	21.251(3)	10.652(2)	14.595(3)	11.788(2)	10.180(2)	9.919(2)	10.087(2)
b [Å]	24.732(3)	12.502(2)	11.488(2)	12.005(2)	11.781(2)	11.382(2)	11.626(2)
c [Å]	6.004(2)	14.036(2)	18.265(4)	27.354(6)	13.508(3)	14.792(3)	14.853(3)
α [°]		64.30(2)		102.47(3)	107.76(3)	98.46(3)	94.46(3)
β [°]		68.56(2)	112.35(3)	93.33(3)	95.73(3)	97.30(3)	103.12(3)
γ [°]		84.36(2)		105.16(3)	114.40(3)	108.41(3)	92.43(3)
V [Å^3]	3155.6(9)	1564.0(6)	2832.4(10)	3621(2)	1356.5(5)	1540.3(5)	1688.0(6)
Z	4	2	4	4	2	2	2
ρ_{calcd} [g cm^{-3}]	1.584	1.505	1.566	1.447	1.659	1.823	1.745
μ [cm^{-1}]	46.26	44.74	49.80	39.11	53.47	46.43	42.42
F(000)	1488	704	1320	1576	668	820	864
$2\theta_{max}$ [°]	51.2	51.1	51.1	51.0	51.1	50.7	50.7
no. unique data	3217	5280	5049	9100	4740	5278	5211
no. obsd. data	2326	4606	3450	5366	4379	4548	4047
no. variables	178	361	334	801	343	424	441
R[a]	0.058	0.038	0.031	0.058	0.034	0.030	0.052
Rw[b]	0.086	0.050	0.075	0.146	0.098	0.071	0.128
residual ρ [e Å^{-3}]	+1.84, −1.86	+0.75, −1.29	+0.44, −1.33	+1.52, −1.36	+1.11, −2.13	+0.57, −2.12	+0.99, −1.72

[a] $R=\Sigma||F_o|-|F_c||/\Sigma|F_o|$. [b] $Rw=\{\Sigma[w(F_o^2-F_c^2)^2]/\Sigma[w(F_o^2)^2]\}^{1/2}$.

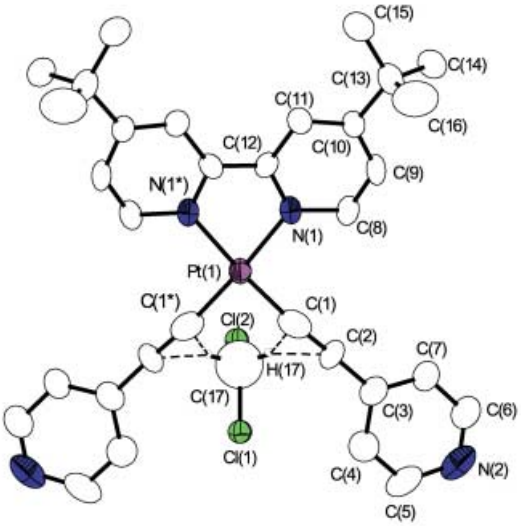

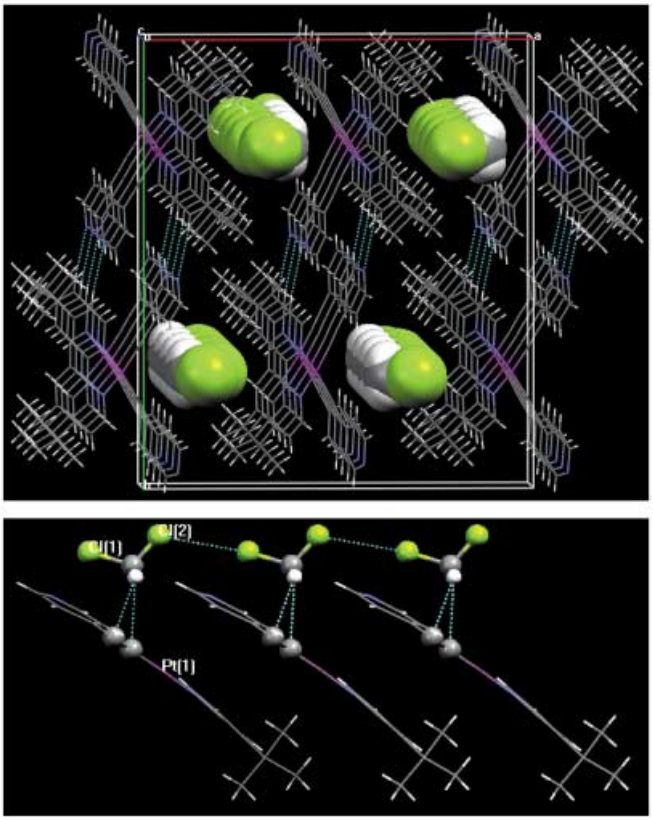

Figure 4. Top: Structure of **1**·CH_2Cl_2 (ORTEP plot; 40% probability ellipsoids), illustrating C–H···π(C≡C) contacts between acetylenic units and CH_2Cl_2 molecule. Selected bond lengths [Å] and angles [°]: Pt(1)–N(1) 2.030(8), Pt(1)–C(1) 1.94(1), C(1)–C(2) 1.22(2); N(1)-Pt(1)-C(1) 97.3(4), N(1)-Pt(1)-C(1*) 175.0(4), Pt(1)-C(1)-C(2) 175.0(10). C–H···π(C≡C) interaction distances [Å] and angles [°]: H(17)–C(1) 2.81, H(17)–C(2) 2.85; C(17)-H(17)-C(1) 129.7, C(17)-H(17)-C2 143.1. Middle: View along the *c* axis of the crystal lattice in **1**·CH_2Cl_2, showing channels containing the $(CH_2Cl_2)_\infty$ chains (space-filling mode), with dashed lines indicating C–H···N(py) interactions. Bottom: Illustration of the $(CH_2Cl_2)_\infty$ chains (ball-and-stick mode) arranged by Cl···Cl interactions along the *b* axis.

tween the bpy 5/5′-H and pyridyl N atoms to afford extended planar sheets.

In the structure of **1**·CH_3CN (Figure 5), each CH_3CN guest is linked to two complex molecules through two weak C–H···π(C≡C) interactions ($d_{H34–C2}=2.79$ Å, $\theta_{C34\text{-}H34\text{-}C2}=150°$; $d_{H33–C9}=2.73$ Å, $\theta_{C34\text{-}H33\text{-}C9}=161°$) to give a 2:2 clathrate. Two types of C–H···N(py) contacts that generate polymeric layers, as found in **1**·CH_2Cl_2, are also apparent, but they are appreciably shorter ($d_{H–N}=2.49$ and 2.63 Å, $\theta_{C–H–N}=169$ and 161°) and no distinct pores are present.

The side-by-side sheetlike motif is also observed in the crystal lattice of **4**·DMF (Figure 6) by C–H···N hydrogen bonding ($d_{H–N}=2.62$–2.67 Å, $\theta_{C\text{-}H\text{-}N}=134$–$158°$) between the 4-pyridylbutadiynyl nitrogen atoms and the five protons of the bpy ligands. The DMF molecule is located between two *tert*-butyl groups, and C–H···O hydrogen bonds ($d_{H–O}=2.38$–2.46 Å, $\theta_{C\text{-}H\text{-}O}=171$–$175°$) are observed with the bpy 6/6′ protons. The acetylenic moieties in **4**·DMF are not involved in hydrogen bonding and channels are not observed running through the lattice.

The molecular structure of **2** (see Supporting Information) depicts interacting dimers resulting from intermolecular C–H···N hydrogen bonding ($d_{H–N}=2.64$ Å, $\theta_{C\text{-}H\text{-}N}=177°$) between the pyridyl 4-proton and the N(py-3) atom of the adjacent molecule; no other short intermolecular contacts are evident. The crystal structure of **5** (see Supporting Information) is generally unremarkable.

The crystal structures of **6** and **6**·CH_3CN exist in the triclinic $P\bar{1}$ space group and the respective bond lengths and angles are similar. Both crystal lattices are also composed of layers of coplanar molecules that are packed into parallel planes (see Supporting Information). The differences between the stacking arrangement of adjacent molecules in **6** and **6**·CH_3CN are depicted in Figure 7. First, the neighboring molecules in **6** are joined by weak C–H···F–C contacts[20] between H28B and H30C atoms of the *tert*-butyl groups and the F5 atom of the pentafluorophenyl moiety ($d_{H–F}=2.55$–2.65 Å, $\theta_{C\text{-}H\text{-}F}=148$–$151°$), but short C–H···F–C contacts are not evident in **6**·CH_3CN. Second, stacked molecules in **6** exhibit overlap in a head-to-tail manner, with the Pt1···Pt_c distance (Figure 7, defined as distance from Pt1 to projection of Pt1* in mean plane of Pt1 molecule) being 3.8 Å, and the shortest Pt···Pt separation (Pt1···Pt1* in Figure 7) at 5.172 Å. In contrast, adjacent molecules in **6**·CH_3CN are displaced (bottom of Figure 7) and significantly longer Pt1···Pt_c (9.4 Å) and Pt···Pt (9.957 Å) separations are observed.

Vapoluminescent performance of film: The apparent ability of complex **1** to signal the presence of CH_2Cl_2 vapor renders it a suitable candidate for VOC sensing applications. A thin film of **1** (thickness ca. 40 μm) on a glass slide, grown from a CH_2Cl_2/Et_2O solution, was prepared in order to study its emission response to VOCs (see Experimental Section). In the absence of organic vapor, the film gave a weak emission at $\lambda_{max} = 527$ nm. Upon introduction of N_2 gas saturated with CH_2Cl_2 vapor, a structured emission at $\lambda_{max} = 520$ nm developed to give a strong "on" signal (Figure 8, top). The emission intensity approached a maximum value after ca. 40 min. Upon purging with nitrogen gas only, the emission

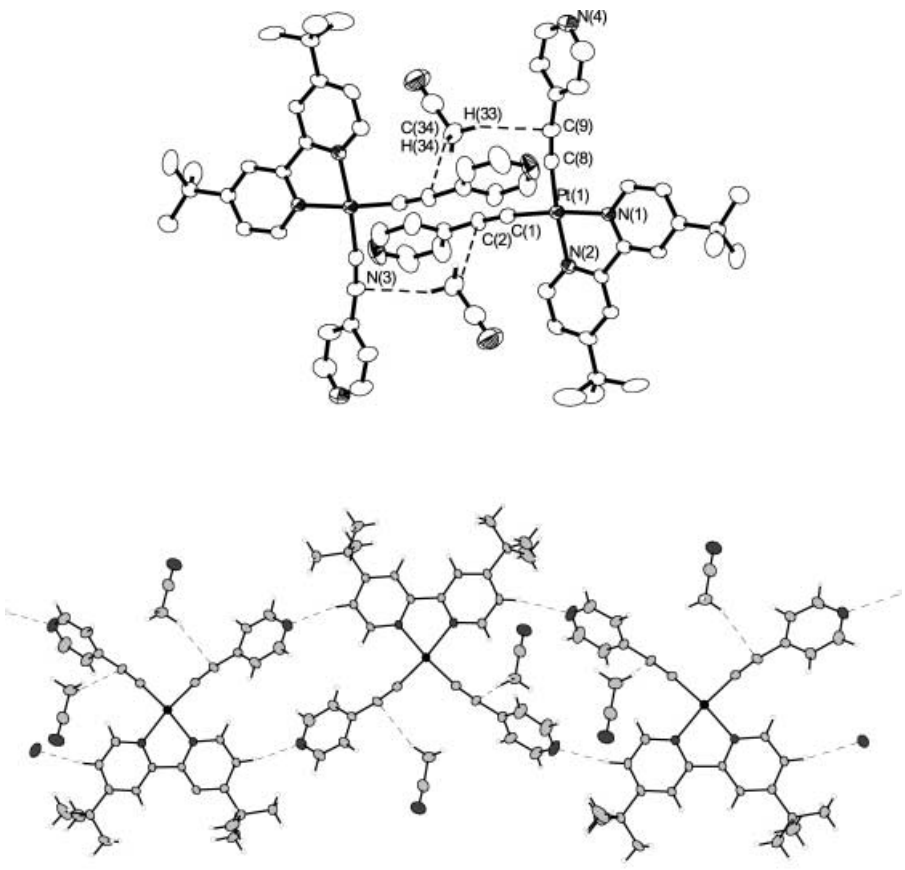

Figure 5. Top: Structure of **1**·CH_3CN (ORTEP plot; 40% probability ellipsoids), illustrating C–H···π(C≡C) interactions between acetylenic units and CH_3CN molecules. Selected bond lengths [Å] and angles [°]: Pt(1)–N(1) 2.063(4), Pt(1)–N(2) 2.078(5), Pt(1)–C(1) 1.962(6), Pt(1)–C(8) 1.947(7), C(1)–C(2) 1.191(9), C(8)–C(9) 1.205(9); N(1)-Pt(1)-C(1) 173.6(2), N(2)-Pt(1)-C(8) 172.4(2), Pt(1)-C(1)-C(2) 175.0(10), Pt(1)-C(8)-C(9) 172.5(5). C–H···π(C≡C) interaction distances [Å] and angles [°]: H(33)–C(9) 2.73, H(34)–C(2) 2.80; C(34)-H(33)-C(9) 150.3, C(34)-H(34)-C(2) 161.4. Bottom: View of an extended layer in **1**·CH_3CN, with dashed lines indicating contacts that are shorter than combined van der Waals radii.

intensity gradually diminished, and was restored to the "off" state after 2 h (inset of Figure 8, top). This procedure was repeated several times to afford the same maximum and minimum intensities, thus indicating the recyclability of the material. No obvious influence was observed when the N_2 carrier gas was replaced by oxygen or air. Significant vapoluminescent behavior was also detected for $CHCl_3$ vapor, but for other VOCs, only minimal (acetonitrile or acetone; see Figure 8, bottom) or negligible (toluene, methanol, or ethanol) response was observed. The emission intensities at 520 nm for various vapor concentrations of CH_2Cl_2 and $CHCl_3$ were measured, and good linearity was obtained (see Supporting Information). The slope of the fitted line for CH_2Cl_2 vapor is larger than that for $CHCl_3$ vapor. Detection limits of 25 and 450 ppm were recorded for CH_2Cl_2 and $CHCl_3$, respectively, under the current experimental set-up.

Discussion

Monomeric and excimeric excited states: Interest in α-diimine platinum(II) bis(acetylide) complexes[21] have increased since the first report on the luminescent properties of [(phen)Pt(C≡CPh)$_2$] by Che and co-workers[15a] and the systematic study by Eisenberg and co-workers.[15b] The lowest-energy transitions of these complexes are generally recognized as ^{3}MLCT transitions [Pt(5d) → π*(α-diimine)], but the involvement of ^{3}IL transitions for derivatives with bis(4-nitrophenylacetylide)[15b,c] or bis(σ-phenylbutadiynyl)[15d] auxiliaries have also been proposed. Recent studies on related luminescent terpyridine/cyclometalated platinum(II)[22] (and α-diimine rhenium(I)[23]) complexes with extended σ-oligoynyl groups, plus theoretical calculations[24] on the α-diimine platinum(II) bis(acetylide) system, suggest that acetylide-to-diimine L′LCT transitions may contribute towards the emissive excited states of this class of complexes. In the present work, we tentatively ascribe the lower-energy band in the absorption spectra of **1**–**6** to an allowed MLCT (L = diimine) transition. This assignment is consistent with the fact that the 350–470 nm band is red shifted by electron-rich acetylide moieties and exhibits negative solvatochromic effects (that is, transition energy increases with greater solvent polarity). Here it is assumed that the energies of nonbonding and weakly π-bonding metal orbitals will increase with the σ-donating strength of the arylacetylide ligands, and that the ground state is more polar than the MLCT excited state.[11c–h] Accordingly, the emissions of **1**–**6** in fluid solution are assigned as ^{3}MLCT [Pt(5d) → π*(α-diimine)] excited states. This assignment is made in view of their solvent-sensitive emission energies and microsecond-regime lifetimes, following the studies of Che, Eisenberg and Schanze's groups.[15]

While the emissive properties of α-diimine platinum(II) bis(acetylide) complexes in fluid and glassy solutions have been systematically investigated,[15] their solid-state behavior remains intriguing.[15d] The emissive behavior of **1**–**6** in solution and rigid matrix closely resembles that of the bis(phenylacetylide) analogue, but the crystallinity-dependent solid-state emissions of **1** and **6** are noteworthy. The intense structured emission in the 460–550 nm range (λ_{max} 517 nm) for crystalline **1**·CH_2Cl_2 at 298 K is comparable in energy to that recorded in CH_2Cl_2, and is similarly assigned to the ^{3}MLCT [Pt(5d) → π*(α-diimine)] excited state of discrete molecules. The relatively weak and significantly diminished emissions of **1**·CH_3CN and the powder form, respectively,

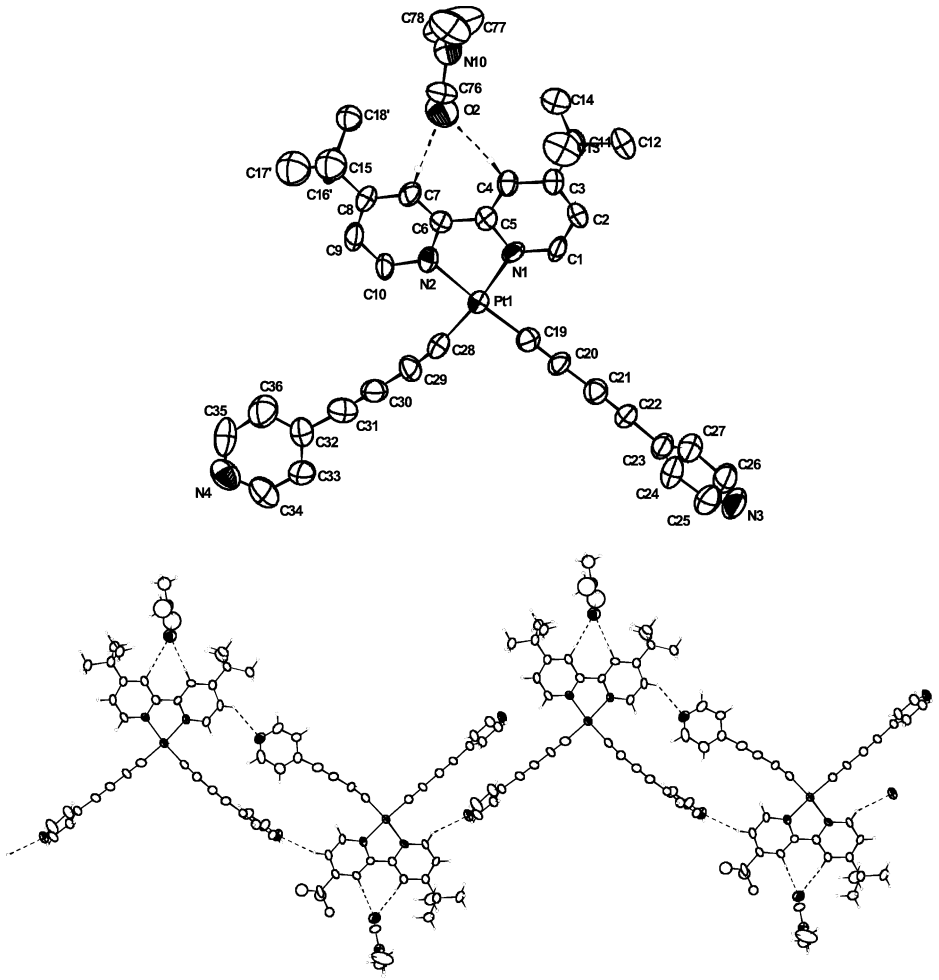

Figure 6. Top: One of the two independent molecules in the crystal **4**·DMF (ORTEP plot; 40% probability ellipsoids). Selected bond lengths [Å] and angles [°]: Pt1–C19 1.946(14), C19–C20 1.199(17), Pt1–C28 1.976(15), C28–C29 1.188(18); N1-Pt1-C28 172.6(5), N2-Pt1-C19 175.4(5), Pt1-C19-C20 173.8(14), Pt1-C28-C29 171.8(13). Bottom: An extended layer of **4**·DMF, with dashed lines indicating contacts that are shorter than combined van der Waals radii.

are red-shifted from that of **1**·CH_2Cl_2 and may be attributed to lumophore aggregation (see later). In contrast, all these forms are highly emissive at 77 K, hence the non-radiative decay processes for these excited molecules are seemingly retarded at low temperatures. For **2**–**5**, the high-energy emissions in the 450–580 nm range and the low-energy structureless emissions at $\lambda_{max} \approx 620$ nm are tentatively assigned to monomeric ^{3}MLCT [Pt(5d)→π*(α-diimine)] and excimeric $^3\pi\pi^*$ states, respectively; the latter is based on previous reports by Miskowski and co-workers.[11a,c]

The structured emission of the green-yellow crystalline form of **6** (obtained from CH_2Cl_2/Et_2O or CH_3CN solution) at 298 K is comparable in energy with that recorded in fluid solution, implying a common monomeric ^{3}MLCT [Pt(5d)→π*(α-diimine)] state for these emissions. The excitation spectra for the green-yellow and orange forms of **6** (left-hand side of Figure 3) exhibit similar absorption cut-off at around 460 nm. The intense emission at $\lambda_{max} = 595$ nm for the orange crystals grown from benzene, which is red-shifted from the ^{3}MLCT emission of discrete [(tBu$_2$bpy)Pt(C≡CC$_6$F$_5$)$_2$] molecules, is tentatively assigned as excimeric $^3\pi\pi^*$ in nature.[11a–c,k] A ^{3}MMLCT (metal-metal-to-ligand charge transfer) assignment is not appropriate since no short Pt–Pt contacts were found in the crystal lattice of **6**. The broad emission at $\lambda_{max} = 620$ nm for the powder form of **6** can be attributed to the existence of significant lumophore aggregation.

Correlation between crystal structures and vapoluminescence: The body of structural data acquired for the complexes in this study has been utilized to interpret their solid-state/thin-film emissive behavior. In particular, the solid-state lattice of the **1**·CH_2Cl_2 crystals and the aforementioned thin film are expected to bear close resemblance because they are recrystallized from the same solvent system. It is proposed that the selectivity of the thin film of **1** is derived from at least 3 components, namely hydrogen-bonding ability, hydrophobicity and size. The extent to which a vapor is sorbed by a material depends largely on the resultant interactions in the solid. The high sorption rate and selectivity for CH_2Cl_2 vapor is thought to arise primarily from the attractive and exoergic interactions produced by the concerted hydrogen bonding between CH_2Cl_2 and the bis(acetylide) unit (the formation of $(CH_2Cl_2)_\infty$ chains via Cl···Cl contacts may also be relevant), which offset the endoergic breaking of intermolecular interactions inherent in the thin film. Accordingly, vapors like CH_3CN with less acidic protons undergo weaker hydrogen bonding; hence sorption is less exoergic and disfavored. However, the neutrality of this material plus the bulky alkyl substituents evidently presents hydrophobic barriers through which polar VOCs such as methanol cannot pass, thus overriding the hydrogen-bonding factor. Finally, consideration of analyte dimensions may be paramount to the observed selectivity of **1**, since crystalline **1**·CH_2Cl_2 was found to be a microporous solid containing channels that harbor the solvent molecules (Figure 4). Thin films of **1** also allow for the sorption of $CHCl_3$ to a lesser degree, and this may be attributed to inferior hydrogen bonding per solvent molecule.

With regards to the sensing/switching mechanism for **1**, we suggest that in the "off" or powder state, lumophore quenching due to C–H···N(py) and/or Pt···N(py) interac-

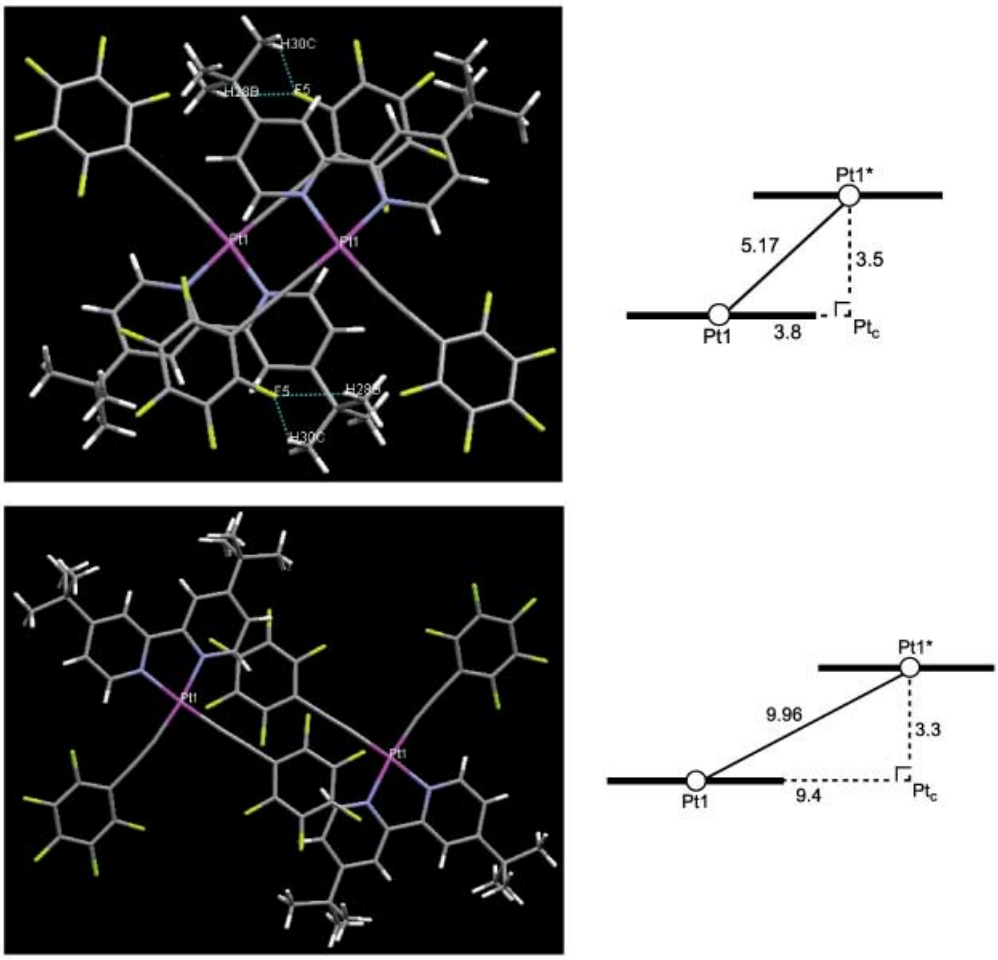

Figure 7. Comparison of overlap between stacked molecules in **6** (top, indicating contacts shorter than combined van der Waals radii) and **6**·CH_3CN (bottom) [Pt1···Pt1* = shortest intermetal separation; Pt1*···Pt_c = interplanar separation; Pt1···Pt_c gives an indication of the extent of intermolecular overlap (in Å; see text for details)].

tions[25] is prevalent, so that only very weak or negligible emission is observed. In the presence of CH_2Cl_2 or $CHCl_3$ vapor, the solvent molecules diffuse into the material where perturbation and expansion of the crystal lattice occurs. This produces sufficient lumophore segregation to trigger intense ^{3}MLCT photoluminescence. This type of lumophore aggregation/quenching is presumably responsible for the weaker solid-state emission of **1**·CH_3CN compared to **1**·CH_2Cl_2, since the C–H···N(py) distances in the former are shorter.

In contrast to material **1**, no vapoluminescent behavior was observed for solids **2**–**5**, even though they are highly luminescent both in crystalline and powder forms. Examination of the crystal lattices of **2**, **4**·DMF, and **5** has revealed no channels that would allow facile sorption and desorption of guest molecules. For the 3-pyridyl analogue **2**, a compact, dimeric arrangement through intermolecular C–H···N(py) interactions is favored. For **4**·DMF, the DMF molecules, and not the bis(4-pyridylbutadiynyl) fragment, are engaged in hydrogen bonding with the α-diimine moiety. This is presumably due to the greater flexibility of the 4-pyridylbutadiynyl group, plus increased electron delocalization leading to weaker C–H···π(C≡C) proton-accepting ability when compared with the 4-pyridylacetylide homologue **1**. Hence the presence of multiple weak interactions and extended pores, plus the interplay between them, demonstrate the uniqueness of crystalline **1** and helps to rationalize the VOC sensing capability for the 4-pyridylacetylide derivative.

The weak C–H···π(C≡C) interactions found in crystals **1**·CH_2Cl_2 and **1**·CH_3CN deserve further comment. In the literature, we have been able to find three crystallographic examples of this type of interaction that were not recognized in the original reports. In the crystal structures of [(*t*Bu_2-bpy)Pt(C≡CPh)$_2$]·CH_2Cl_2 and [(4,7-diphenyl-2,2-bipyridine)Pt(C≡CPh)$_2$]·CH_2Cl_2,[15d] the solvated CH_2Cl_2 molecules weakly interact with the bis(acetylide) unit with C–H···π distances of 2.64–2.97 Å. In the crystal lattice of [(*t*Bu_2-bpy)Pt(C≡CC_6H_4-4-CH_3)$_2$]·$CHCl_3$ (see Supporting Information for schematic depiction),[26] the $CHCl_3$ molecule weakly coordinates to the bis(acetylide) fragment with C–H···π distances in the 2.68–3.04 Å range. This last example can be regarded as evidence to support the capability of complex **1** to bind a chloroform molecule, since crystalline **1** exhibited a response in the presence of $CHCl_3$ vapor.

In the crystal structure of **6**·CH_3CN, intermolecular C–H···F–C interactions and π stacking of aryl groups between layers of lumophore molecules are not observed. For unsol-

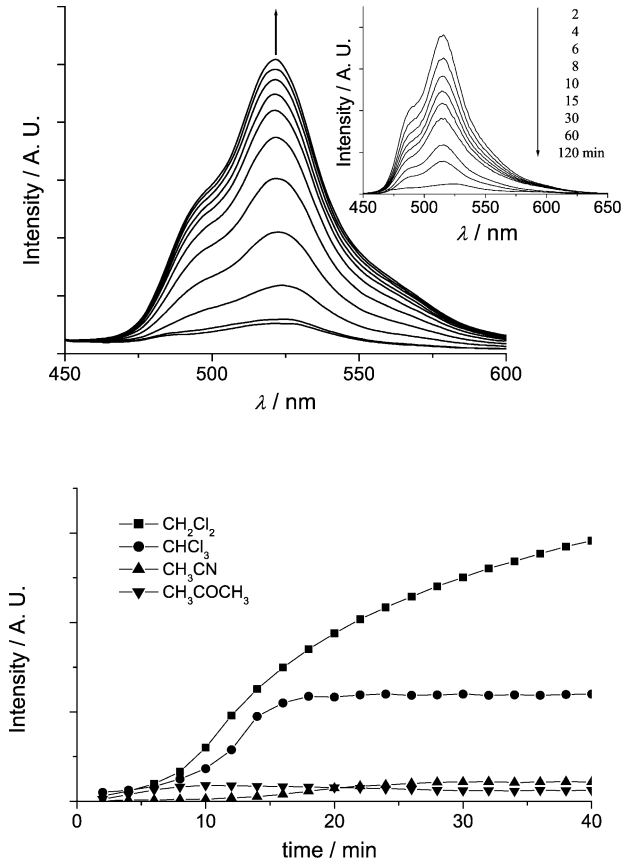

Figure 8. Top: Emission spectral traces for a film prepared with **1** in the presence of N_2 saturated with CH_2Cl_2 vapor ($\lambda_{ex}=350$ nm, N_2 flow rate = 12 mL min^{-1}, interval = 2 min). [Inset: Emission spectral traces for this film upon removal of CH_2Cl_2 vapor (N_2 flow rate = 90 mL min^{-1})]. Bottom: Relative emission intensity (monitored at 520 nm) versus time for this film upon exposure to N_2 saturated with VOC vapors.

vated **6**, the significantly shorter Pt1···Pt_c separation (see Figure 7) of 3.8 Å for adjacent molecules, compared to that in **6**·CH_3CN (9.4 Å), clearly indicates a superior degree of intermolecular overlap. Hence it is evident that weak interplanar C–H···F–C contacts and effective π overlap of aromatic rings play a key role in the overall packing arrangement of individual lumophores in these solids. The binding energy for each C–H···F–C linkage (calculated as 2.2 kJ mol^{-1} for the difluoromethane dimer in the gas phase[20c]) should be lower than the bond energy for more traditional hydrogen-bonding interactions such as O–H···F–C (8.7 kJ mol^{-1} for difluoromethane·H_2O[20c]). We suggest that the sorption of solvent molecules into the crystal lattice of **6** can influence the intermolecular interactions (i.e. π stacking and C–H···F–C) and therefore perturb the emission properties of the lumophores. Due to the disorder of the *tert*-butyl groups in the crystal structure of **6**·CH_3CN, we cannot accurately evaluate this effect at this stage. The emission at λ_{max} = 595 nm for the unsolvated orange form of **6**, obtained from benzene, is proposed to arise from the overlap of neighboring lumophore layers, since the interplanar distance of ≈3.5 Å resembles typical π-stacking distances (3.3–3.6 Å).[27] We have recently highlighted contrasting π-stacking conformations and different solid-state emissive properties for solvated and unsolvated luminescent organoplatinum(II) complexes.[11k]

Conclusion

A comparison of crystal structures and vapoluminescent behavior has provided valuable information regarding host–guest, host–host and guest–guest interactions in this vapor-sensing system. Significantly, metal–metal interactions are not involved in the VOC sensing ability of these materials, which is different from recent reports on platinum(II)- and gold(I)-based vapoluminescent solids. Generally, several factors appear to be crucial to the vapoluminescence of materials **1** and **6**. First, the *tert*-butyl groups on the bpy ligand not only impart solubility to the complexes to facilitate their synthesis, but also inhibit short Pt–Pt interactions between individual lumophores. Second, the bis(acetylide) fragment, as observed in **1**·CH_2Cl_2, functions as the receptor berth for CH_2Cl_2 and $CHCl_3$ molecules through multiple weak C–H···π(C≡C) interactions. Cl···Cl contacts are also observed to connect guest CH_2Cl_2 molecules together into continuous $(CH_2Cl_2)_\infty$ chains. These noncovalent interactions control the vapoluminescent selectivity of crystalline **1** towards CH_2Cl_2 and $CHCl_3$ vapors. Third, a contrast in emission output due to lumophore aggregation accounts for the different vapoluminescent behavior exhibited by crystalline **1** and **6**. While **1** shows switch-on luminescence towards CH_2Cl_2 vapor, **6** is interconverted between two "on" states, namely monomeric and excimeric emissions, for vapor sorption and desorption, respectively.

In summary, the origin of the vapoluminescent responses for complexes **1** and **6** is the highly environment-sensitive nature of the [(α-diimine)Pt^{II}] lumophore coupled efficiently with the hydrogen-bonding affinity of the functionalized bis(acetylenic) fragment. Weak noncovalent interactions [for example, C–H···π(C≡C), C–H···N(py), π-π, Cl···Cl, and C–H···F–C] apparently orchestrate the reversible sensing processes. This design paradigm may be beneficial to the future development of porous metal-based luminescent sensors.

Experimental Section

General remarks: All starting materials were purchased from commercial sources and used as received unless stated otherwise. The solvents used for synthesis were of analytical grade. The compounds 4-ethynylpyridine,[28] 3-ethynylpyridine,[28] 2-ethynylpyridine,[28] 2-ethynylthiophene,[29] 4-butadiynylpyridine,[30] pentafluorophenylacetylene[31] and [(tBu$_2$-bpy)$PtCl_2$][26] were prepared according to literature methods. ^{1}H and ^{13}C (Bruker Avance 400 or 300 DRX FT-NMR spectrometer; referenced to residual solvent) and ^{19}F (Bruker Avance 400; trifluoroacetic acid reference) NMR spectra were recorded at 298 K. Mass spectra (FAB) were obtained on a Finnigan MAT 95 mass spectrometer. Elemental analyses were performed by Beijing Institute of Chemistry, Chinese Academy of Sciences.

UV/Vis absorption spectra were obtained on a Perkin-Elmer Lambda 19 UV-visible spectrophotometer. Steady-state emission spectra were recorded on a SPEX 1681 Fluorolog-2 series F111 spectrophotometer equipped with a Hamamatsu R928 PMT detector. Emission lifetimes were performed with a Quanta Ray DCR-3 pulsed Nd:YAG laser system (pulse output 355 nm, 8 ns). Errors for λ(±1 nm), τ (±10%), and ϕ (±

10%) values are estimated. Details of solvent treatment for photophysical studies, instrumentation and emission measurements have been given previously.[11i]

Syntheses of complexes 1–6: A mixture of [(*t*Bu$_2$bpy)PtCl$_2$] (0.18 g, 0.34 mmol), the corresponding aromatic acetylene (1.0 mmol), diisopropylamine (3 mL), and CuI (5 mg) in degassed dichloromethane (30 mL) was stirred for 24 h under a nitrogen atmosphere at room temperature in the absence of light. The resultant yellow solution was evaporated to dryness. The crude product was purified by flash chromatography (neutral Al_2O_3, CH_2Cl_2 as eluent) and recrystallized from dichloromethane/diethyl ether.

[(*t*Bu$_2$bpy)Pt(C≡C-4-py)$_2$] (1): yield: 0.20 g, 88%; ^{1}H NMR (300 MHz, $CDCl_3$): δ = 9.56 (d, J = 6.0 Hz, 2H), 8.46 (d, J = 4.6 Hz, 4H), 7.99 (s, 2H), 7.63 (d, J = 6.0 Hz, 2H), 7.35 (d, J = 4.6 Hz, 4H), 1.45 ppm (s, 18H); ^{13}C{^{1}H} NMR (100 MHz, CD_2Cl_2): δ = 166.1, 157.9, 152.4, 151.0, 137.4, 127.9, 126.6, 121.1, 101.3, 97.0, 37.5, 31.6 ppm; IR (Nujol): $\tilde{\nu}$ = 2116, 2128 cm^{-1} (C≡C); FAB MS: m/z: 668 [M^+]; elemental analysis calcd (%) for $PtC_{32}H_{32}N_4{\cdot}CH_2Cl_2$: C 52.66, H 4.55, N 7.44; found: C 52.83, H 4.54, N 7.05.

[(*t*Bu$_2$bpy)Pt(C≡C-3-py)$_2$] (2): yield: 0.17 g, 75%; ^{1}H NMR (300 MHz, $CDCl_3$): δ = 9.64 (d, J = 6.0 Hz, 2H), 8.74 (s, 2H), 8.35 (d, J = 4.8 Hz, 2H), 7.97 (s, 2H), 7.77 (d, J = 6.0 Hz, 2H), 7.61 (d, J = 6.0 Hz, 2H), 7.16 (dd, J = 7.8 Hz, J = 4.8 Hz, 2H), 1.45 ppm (s, 18H); FAB MS: m/z: 668 [M^+]; elemental analysis calcd (%) for $PtC_{32}H_{32}N_4$: C 57.56, H 4.83, N 8.39; found: C 57.50, H 4.99, N 8.39.

[(*t*Bu$_2$bpy)Pt(C≡C-2-py)$_2$] (3): yield: 0.16 g, 70%; ^{1}H NMR (300 MHz, $CDCl_3$): δ = 9.49 (d, J = 5.9 Hz, 2H), 8.53 (d, J = 4.8 Hz, 2H), 8.27 (s, 2H), 7.54 (td, ^2J = 7.6 Hz, ^3J = 1.8 Hz, 2H), 7.48–7.43 (m, 4H), 7.05 (m, 2H), 1.37 ppm (s, 18H); FAB MS: m/z: 668 [M^+]; elemental analysis calcd (%) for $PtC_{32}H_{32}N_4$: C 57.56, H 4.83, N 8.39; found: C 56.70, H 4.83, N 8.10.

[(*t*Bu$_2$bpy)Pt(C≡C–C≡C-4-py)$_2$] (4): yield: 0.20 g, 82%; ^{1}H NMR (300 MHz, CD_2Cl_2): δ = 9.00 (d with ^{195}Pt satellites, J = 6.0 Hz, J(Pt,H) = 40.0 Hz, 2H), 8.53 (d with ^{195}Pt satellites, J = 5.8 Hz, J(Pt,H) = 40.0 Hz, 4H), 8.13 (s with ^{195}Pt satellites, J(Pt,H) = 40.6 Hz, 2H), 7.57 (d with ^{195}Pt satellites, J = 6.0 Hz, J(Pt,H) = 40.4 Hz, 2H), 7.34 (d with ^{195}Pt satellites, J = 4.6 Hz, J(Pt,H) = 40.0 Hz, 4H), 1.52 ppm (s, 18H); ^{13}C{^{1}H} NMR (100 MHz, CD_2Cl_2): δ = 166.1, 158.2, 152.0, 151.3, 133.7, 128.0, 126.4, 122.1, 93.1, 84.6, 84.0, 68.9, 37.6, 31.8 ppm; FAB MS: m/z: 716 [M^+]; elemental analysis calcd (%) for $PtC_{36}H_{32}N_4$: C 60.41, H 4.51, N 7.83; found: C 60.46, H 4.50, N 7.75.

[(*t*Bu$_2$bpy)Pt(C≡C-2-thienyl)$_2$] (5): yield: 0.11 g, 48%; ^{1}H NMR (300 MHz, $CDCl_3$): δ = 9.53 (d, J = 5.6 Hz, 2H), 7.97 (s, 2H), 7.54 (d, J = 4.5 Hz, 2H), 7.09 (d, J = 3.4 Hz, 2H), 7.03 (d, J = 5.1 Hz, 2H), 6.91 (m, 2H), 1.44 ppm (s, 18H); FAB MS: 678 (M^+); elemental analysis calcd (%) for $PtC_{30}H_{30}N_2S_2$: C 53.16, H 4.46, N 4.13; found: C 53.64, H 4.50, N 3.80.

[(*t*Bu$_2$bpy)Pt(C≡CC$_6$F$_5$)$_2$] (6): The product was recrystallized from hot benzene. Yield: 0.25 g, 87%; ^{1}H NMR (300 MHz, $CDCl_3$): δ = 9.60 (d, J = 4.5 Hz, 2H), 7.99 (s, 2H), 7.60 (d, J = 4.5 Hz, 2H), 1.46 ppm (s, 18H); ^{19}F{^{1}H} NMR (376 MHz, $CDCl_3$): δ = −138.6 (dd, ^3J = 22.6 Hz, ^4J = 7.5 Hz, 4F), −159.4 (t, ^3J = 22.6 Hz, 2F), −164.4 ppm (td, ^3J = 22.6 Hz, ^4J = 7.5 Hz, 4F); FAB MS: m/z: 846 [M^+]; elemental analysis calcd (%) for $PtC_{34}H_{24}F_{10}N_2{\cdot}C_6H_6$: C 52.01, H 3.27, N 3.03; found: C 52.33, H 3.50, N 3.12.

X-ray crystallography: Data were collected on a MAR diffractometer with a 300 mm image plate detector using monochromatized $Mo_{K\alpha}$ radiation (λ = 0.71071 Å). The images were interpreted and intensities integrated by using program DENZO.[32]

For **1**·CH_2Cl_2 and **1**·CH_3CN, the structures were solved by Patterson methods, expanded by Fourier methods (PATTY),[33] and refined by full-matrix least-squares using the software package TeXsan[34] on a Silicon Graphics Indy computer. In the least-square refinement, all non-hydrogen atoms were refined anisotropically (the non-hydrogen atoms of the solvent molecule in **1**·CH_2Cl_2 have large thermal parameters and were refined isotropically), and all H atoms at calculated positions with thermal parameters equal to 1.3 times that of the attached C atoms were not refined. For **1**·CH_2Cl_2, one crystallographic asymmetric unit consists of half of one formula unit with Pt(1) and the non-hydrogen atoms of the solvent molecule at special positions. For **1**·CH_3CN, one crystallographic asymmetric unit consists of one formula unit.

For **2**, **4**·DMF, **5**, **6**, and **6**·CH_3CN, the structures were solved by direct methods employing SIR-97[35] program on PC. The Pt and many hydrogen atoms were located according to direct methods and successive least-square Fourier cycles. Positions of other non-hydrogen atoms were found after successful refinement by full-matrix least-squares using the program SHELXL-97[36] on a PC. In the final stage of least-square refinement, all non-H atoms were refined anisotropically. The positions of H atoms were calculated based on riding mode with thermal parameters equal to 1.2 times that of the associated C atoms, and participated in the calculation of final R indices. One crystallographic asymmetric unit consists of one formula unit, with the exception of **4**·DMF where one crystallographic asymmetric unit consists of two formula units.

CCDC-188713–188717 (**1**·CH_2Cl_2, **1**·CH_3CN, **2**, **4**·DMF, and **5**, respectively) and CCDC-214726 (**6**) CCDC-214727 (**6**·CH_3CN) contain the supplementary crystallographic data for the this paper. These data can be obtained free of charge via www.ccdc.cam.ac.uk/conts/retrieving.html (or from the Cambridge Crystallographic Data Centre, 12 Union Road, Cambridge CB2 1EZ, UK; fax: (+44) 1223-336-033; or deposit@ccdc.cam.ac.uk).

Film preparation and determination of emission response: Complex **1** (20 mg) was dissolved in CH_2Cl_2 (20 mL) in a beaker. A piece of glass slide (2 cm × 2 cm), pretreated by HF solution, was placed on the bottom of the complex solution. Diethyl ether vapor was allowed to diffuse slowly into this solution. After 20–30 h, the glass slide with a microcrystalline layer of **1** on the surface was removed and used for subsequent measurements. The thickness of the film was determined by SEM to be around 40 μm.

A diagram showing the set-up for determining the emission response of the sensing film towards VOCs is shown in the Supporting Information. Organic vapors of various concentrations were produced by the diffusion tube method.[37] The N_2 gas containing the organic vapor was fed into a flow cell in which the sensing film was exposed to the gas stream. The glass slide was orientated to face the excitation light source in the spectrofluorometer (Perkin–Elmer LS-50B).

Acknowledgement

We are grateful for financial support from The University of Hong Kong, the Research Grants Council of Hong Kong SAR, China [HKU 7077/01P] and Area of Excellence Scheme (AoE/P-10/01), Unversity Grants Committee of HK SAR, China. We thank Dr. Kung-Kai Cheung for solving some of the crystal structures.

[1] a) T. E. Müller, D. M. P. Mingos, D. J. Williams, *J. Chem. Soc. Chem. Commun.* **1994**, 1787–1788; b) T. Steiner, M. Tamm, *J. Organomet. Chem.* **1998**, *570*, 235–239; c) T. Steiner, E. B. Starikov, A. M. Amado, J. J. C. Teixeira-Dias, *J. Chem. Soc. Perkin Trans. 2* **1995**, 1321–1326.

[2] For vapoluminescent polymeric/organic compounds, see: a) J. S. Yang, T. M. Swager, *J. Am. Chem. Soc.* **1998**, *120*, 11864–11873; b) S. Content, W. C. Trogler, M. J. Sailor, *Chem. Eur. J.* **2000**, *6*, 2205–2213; c) M. Schlupp, T. Weil, A. J. Berresheim, U. M. Wiesler, J. Bargon, K. Müllen, *Angew. Chem.* **2001**, *113*, 4124–4129; *Angew. Chem. Int. Ed.* **2001**, *40*, 4011–4015; d) B. K. An, S. K. Kwon, S. D. Jung, S. Y. Park, *J. Am. Chem. Soc.* **2002**, *124*, 14410–14415; e) Z. Fei, N. Kocher, C. J. Mohrschladt, H. Ihmels, D. Stalke, *Angew. Chem.* **2003**, *115*, 807–811; *Angew. Chem. Int. Ed.* **2003**, *42*, 783–787; f) S. W. Zhang, T. M. Swager, *J. Am. Chem. Soc.* **2003**, *125*, 3420–3421; for examples of vapochromic solids, see: g) M. Albrecht, M. Lutz, A. L. Spek, G. van Koten, *Nature* **2000**, *406*, 970–974; h) L. G. Beauvais, M. P. Shores, J. R. Long, *J. Am. Chem. Soc.* **2000**, *122*, 2763–2772; i) E. J. Fernández, J. M. López-de-Luzuriaga, M. Monge, M. E. Olmos, J. Pérez, A. Laguna, A. A. Mohamed, J. P. Fackler, Jr., *J. Am. Chem. Soc.* **2003**, *125*, 2022–2023.

[3] a) M. H. Keefe, K. D. Benkstein, J. T. Hupp, *Coord. Chem. Rev.* **2000**, *205*, 201–228; b) J. N. Demas, B. A. DeGraff, *Coord. Chem. Rev.* **2001**, *211*, 317–351.

[4] a) K. A. Van Houten, D. C. Heath, R. S. Pilato, *J. Am. Chem. Soc.* **1998**, *120*, 12359–12360; b) J. Pang, E. J. P. Marcotte, C. Seward, R. S. Brown, S. Wang, *Angew. Chem.* **2001**, *113*, 4166–4169; *Angew. Chem. Int. Ed.* **2001**, *40*, 4042–4045; c) M. Kato, A. Omura, A. Toshikawa, S. Kishi, Y. Sugimoto, *Angew. Chem.* **2002**, *114*, 3315–3317; *Angew. Chem. Int. Ed.* **2002**, *41*, 3183–3185; d) M. A. Rawashdeh-Omary, M. A. Omary, J. P. Fackler, Jr., *J. Am. Chem. Soc.* **2001**, *123*, 9689–9691.

[5] a) R. V. Slone, J. T. Hupp, C. L. Stern, T. E. Albrecht-Schmitt, *Inorg. Chem.* **1996**, *35*, 4096–4097; b) R. V. Slone, J. T. Hupp, *Inorg. Chem.* **1997**, *36*, 5422–5423; c) K. D. Benkstein, J. T. Hupp, C. L. Stern, *Angew. Chem.* **2000**, *112*, 3013–3015; *Angew. Chem. Int. Ed.* **2000**, *39*, 2891–2893; d) S. S. Sun, A. J. Lees, *Coord. Chem. Rev.* **2002**, *230*, 171–192; e) S. S. Sun, A. J. Lees, *J. Am. Chem. Soc.* **2000**, *122*, 8956–8967; f) S. S. Sun, J. A. Anspach, A. J. Lees, P. Y. Zavalij, *Organometallics* **2002**, *21*, 685–693.

[6] a) C. T. Lin, N. Sutin, *J. Phys. Chem.* **1976**, *80*, 97–105; b) G. Dimarco, M. Lanza, S. Campagna, *Adv. Mater.* **1995**, *7*, 468–471; c) W. Y. Xu, K. A. Kneas, J. N. Demas, B. A. DeGraff, *Anal. Chem.* **1996**, *68*, 2605–2609; d) G. Dimarco, M. Lanza, M. Pieruccini, S. Campagna, *Adv. Mater.* **1996**, *8*, 576–580; e) X. M. Li, K. Y. Wong, *Anal. Chim. Acta* **1992**, *262*, 27–32; f) W. W. S. Lee, K. Y. Wong, X. M. Li, *Anal. Chem.* **1993**, *65*, 255–258; g) A. Mills, A. Lepre, B. R. C. Theobald, E. Slade, B. A. Murrer, *Anal. Chem.* **1997**, *69*, 2842–2847; h) D. M. Papkovsky, G. V. Ponomarev, W. Trettnak, P. O'Leary, *Anal. Chem.* **1995**, *67*, 4112–4117; i) C. M. Che, W. F. Fu, S. W. Lai, Y. J. Hou, Y. L. Liu, *Chem. Commun.* **2003**, 118–119.

[7] a) J. C. Vickery, M. M. Olmstead, E. Y. Fung, A. L. Balch, *Angew. Chem.* **1997**, *109*, 1227–1229; *Angew. Chem. Int. Ed. Engl.* **1997**, *36*, 1179–1181; b) M. M. Olmstead, F. Jiang, S. Attar, A. L. Balch, *J. Am. Chem. Soc.* **2001**, *123*, 3260–3267.

[8] a) M. A. Mansour, W. B. Connick, R. J. Lachicotte, H. J. Gysling, R. Eisenberg, *J. Am. Chem. Soc.* **1998**, *120*, 1329–1330; b) Y. A. Lee, J. E. McGarrah, R. J. Lachicotte, R. Eisenberg, *J. Am. Chem. Soc.* **2002**, *124*, 10662–10663.

[9] a) C. A. Daws, C. L. Exstrom, J. R. Sowa Jr. , K. R. Mann, *Chem. Mater.* **1997**, *9*, 363–368; b) C. E. Buss, C. E. Anderson, M. K. Pomije, C. M. Lutz, D. Britton, K. R. Mann, *J. Am. Chem. Soc.* **1998**, *120*, 7783–7790; c) S. M. Drew, D. E. Janzen, C. E. Buss, D. I. MacEwan, K. M. Dublin, K. R. Mann, *J. Am. Chem. Soc.* **2001**, *123*, 8414–8415; d) C. E. Buss, K. R. Mann, *J. Am. Chem. Soc.* **2002**, *124*, 1031–1039.

[10] a) E. Cariati, J. Bourassa, P. C. Ford, *Chem. Commun.* **1998**, 1623–1624; b) E. Cariati, X. Bu, P. C. Ford, *Chem. Mater.* **2000**, *12*, 3385–3391.

[11] a) V. M. Miskowski, V. H. Houlding, *Inorg. Chem.* **1989**, *28*, 1529–1533; b) V. M. Miskowski, V. H. Houlding, *Inorg. Chem.* **1991**, *30*, 4446–4452; c) V. H. Houlding, V. M. Miskowski, *Coord. Chem. Rev.* **1991**, *111*, 145–152; d) V. M. Miskowski, V. H. Houlding, C. M. Che, Y. Wang, *Inorg. Chem.* **1993**, *32*, 2518–2524; e) J. A. Bailey, V. M. Miskowski, H. B. Gray, *Inorg. Chem.* **1993**, *32*, 369–370; f) J. A. Bailey, M. G. Hill, R. E. Marsh, V. M. Miskowski, W. P. Schaefer, H. B. Gray, *Inorg. Chem.* **1995**, *34*, 4591–4599; g) S. D. Cummings, R. Eisenberg, *J. Am. Chem. Soc.* **1996**, *118*, 1949–1960; h) R. Büchner, C. T. Cunningham, J. S. Field, R. J. Haines, D. R. McMillin, G. C. Summerton, *J. Chem. Soc. Dalton Trans.* **1999**, 711–717; i) S. W. Lai, M. C. W. Chan, T. C. Cheung, S. M. Peng, C. M. Che, *Inorg. Chem.* **1999**, *38*, 4046–4055; j) J. DePriest, G. Y. Zheng, N. Goswami, D. M. Eichhorn, C. Woods, D. P. Rillema, *Inorg. Chem.* **2000**, *39*, 1955–1963; k) W. Lu, M. C. W. Chan, K. K. Cheung, C. M. Che, *Organometallics* **2001**, *20*, 2477–2486; l) W. Lu, N. Zhu, C. M. Che, *Chem. Commun.* **2002**, 900–901; m) V. W. W. Yam, K. M. C. Wong, N. Zhu, *J. Am. Chem. Soc.* **2002**, *124*, 6506–6507.

[12] a) H. Q. Liu, T. C. Cheung, S. M. Peng, C. M. Che, *J. Chem. Soc. Chem. Commun.* **1995**, 1787–1788; b) L. Z. Wu, T. C. Cheung, C. M. Che, K. K. Cheung, M. H. W. Lam, *Chem. Commun.* **1998**, 1127–1128; c) K. H. Wong, M. C. W. Chan, C. M. Che, *Chem. Eur. J.* **1999**, *5*, 2845–2849; d) C. M. Che, J. L. Zhang, L. R. Lin, *Chem. Commun.* **2002**, 2556–2557; e) C. M. Che, W. F. Fu, S. W. Lai, Y. J. Hou, Y. L. Liu, *Chem. Commun.* **2003**, 118–119; f) L. Monsú Scolaro, A. Romeo, A. Terracina, *Chem. Commun.* **1997**, 1451–1452; g) C. S. Peyratout, T. K. Aldridge, D. K. Crites, D. R. McMillin, *Inorg. Chem.* **1995**, *34*, 4484–4489.

[13] a) M. A. Mortellaro, D. G. Nocera, *J. Am. Chem. Soc.* **1996**, *118*, 7414–7415; b) M. A. Mortellaro, D. G. Nocera, *ChemTech* **1996**, *26*, 17–23.

[14] a) Y. Fujikura, K. Sonogashira, N. Hagihara, *Chem. Lett.* **1975**, 1067–1070; b) C. J. Adams, S. L. James, P. R. Raithby, *Chem. Commun.* **1997**, 2155–2156.

[15] a) C. W. Chan, L. K. Cheng, C. M. Che, *Coord. Chem. Rev.* **1994**, *132*, 87–97; b) M. Hissler, W. B. Connick, D. K. Geiger, J. E. McGarrah, D. Lipa, R. J. Lachicotte, R. Eisenberg, *Inorg. Chem.* **2000**, *39*, 447–457; c) C. E. Whittle, J. A. Weinstein, M. W. George, K. S. Schanze, *Inorg. Chem.* **2001**, *40*, 4053–4062; d) S. C. Chan, M. C. W. Chan, C. M. Che, Y. Wang, K. K. Cheung, N. Zhu, *Chem. Eur. J.* **2001**, *7*, 4180–4190.

[16] a) A. Bondi, *J. Phys. Chem.* **1964**, *68*, 441–451; b) T. Takagi, A. Tanaka, S. Matsuo, H. Maezaki, M. Tani, H. Fujiwara, Y. Sasaki, *J. Chem. Soc. Perkin Trans. 2* **1987**, 1015–1018.

[17] L. Brunel, F. Carré, S. G. Dutremez, C. Guérin, F. Dahan, O. Eisenstein, G. Sini, *Organometallics* **2001**, *20*, 47–54.

[18] For examples of Cl···Cl interactions and their application in crystal engineering, see: a) J. A. R. P. Sharma, G. R . Desiraju, *Acc. Chem. Res.* **1986**, *19*, 222–228; b) N. Ramasubbu, R. Parthasarathy, P. Murray-Rust, *J. Am. Chem. Soc.* **1986**, *108*, 4308–4314; c) G. R. Desiraju, R. Parthasarathy, *J. Am. Chem. Soc.* **1989**, *111*, 8725–8726; d) J. N. Moorthy, R. Natarajan, P. Mal, P. Venugopalan, *J. Am. Chem. Soc.* **2002**, *124*, 6530–6531.

[19] a) G. R. Desiraju, *Crystal Engineering*, T*he Design of Organic Solids*, Elsevier, Amsterdam, **1989**; b) G. R. Desiraju, T. Steiner, *The Weak Hydrogen Bond in Structural Chemistry and Biology*, Oxford University, New York, **1999**; c) I. Alkorta, I. Rozas, J. Elguero, *Chem. Soc. Rev.* **1998**, *27*, 163–170.

[20] a) H. C. Weiss, R. Boese, H. L. Smith, M. M. Haley, *Chem. Commun.* **1997**, 2403–2404; b) V. R. Thalladi, H. C. Weiss, D. Bläser, R. Boese, A. Nangia, G. R. Desiraju, *J. Am. Chem. Soc.* **1998**, *120*, 8702–8710; c) W. Caminati, S. Melandri, P. Moreschini, P. G. Favero, *Angew. Chem.* **1999**, *111*, 3105–3107; *Angew. Chem. Int. Ed.* **1999**, *38*, 2924–2925; d) J. Parsch, J. W. Engels, *J. Am. Chem. Soc.* **2002**, *124*, 5664–5672; e) S. C. F. Kui, N. Zhu, M. C. W. Chan, *Angew. Chem.* **2003**, *115*, 1666–1670; *Angew. Chem. Int. Ed.* **2003**, *42*, 1628–1632.

[21] a) W. B. Connick, D. P. Geiger, R. Eisenberg, *Inorg. Chem.* **1999**, *38*, 3264–3265; b) J. E. McGarrah, Y. J. Kim, M. Hissler, R. Eisenberg, *Inorg. Chem.* **2001**, *40*, 4510–4511; c) I. E. Pomestchenko, C. R. Luman, M. Hissler, R. Ziessel, F. N. Castellano, *Inorg. Chem.* **2003**, *42*, 1394–1396; d) S. Fernandez, J. Fornies, B. Gil, J. Gomez, E. Lalinde, *J. Chem. Soc. Dalton Trans.* **2003**, 822–830.

[22] a) V. W. W. Yam, R. P. L. Tang, K. M. C. Wong, K. K. Cheung, *Organometallics* **2001**, *20*, 4476–4482; b) W. Lu, B. X. Mi, M. C. W. Chan, Z. Hui, N. Zhu, S. T. Lee, C. M. Che, *Chem. Commun.* **2002**, 206–207; c) Q. Z. Yang, L. Z. Wu, Z. X. Wu, L. P. Zhang, C. H. Tung, *Inorg. Chem.* **2002**, *41*, 5653–5655; d) V. W. W. Yam, K. M. C. Wong, N. Zhu, *Angew. Chem.* **2003**, *115*, 1438–1441; *Angew. Chem. Int. Ed.* **2003**, *42*, 1400–1403.

[23] V. W. W. Yam, S. H. F. Chong, C. C. Ko, K. K. Cheung, *Organometallics* **2000**, *19*, 5092–5097.

[24] a) A. Klein, J. van Slageren, S. Záli, *Inorg. Chem.* **2002**, *41*, 5216–5225; b) J. van Slageren, A. Klein, S. Záli, *Coord. Chem. Rev.* **2002**, *230*, 193–211.

[25] J. H. K. Yip, Suwarno, J. J. Vittal, *Inorg. Chem.* **2000**, *39*, 3537–3543.

[26] C. J. Adams, S. L. James, X. Liu, P. R. Raithby, L. J. Yellowlees, *J. Chem. Soc. Dalton Trans.* **2000**, 63–67.

[27] C. A. Hunter, J. K. M. Sanders, *J. Am. Chem. Soc.* **1990**, *112*, 5525–5534.

[28] J. G. Rodríguez, R. Martin-Villamil, F. H. Cano, I. Fonseca, *J. Chem. Soc. Perkin Trans. 1* **1997**, 709–714.

[29] R. Wu, J. S. Schumm, D. L. Pearson, J. M. Tour, *J. Org. Chem.* **1996**, *61*, 6906–6921.

[30] R. Ziessel, J. Suffert, M. T. Youinou, *J. Org. Chem.* **1996**, *61*, 6535–6546.

[31] Y. D. Zhang, J. X. Wen, *Synthesis* **1990**, 727–728.

[32] DENZO in D. Gewirth, with the cooperation of the program authors Z. Otwinowski, and W. Minor, *The HKL Manual - A description of programs DENZO, XDISPLAYF and SCALEPACK*, Yale University, New Haven, **1995**.
[33] PATTY in P. R. Beurskens, G. Admiraal, W. P. Bosman, S. Garcia-Granda, R. O. Gould, J. M. M. Smits, C. Smykalla, *The DIRDIF program system*, Technical Report of the Crystallography Laboratory, University of Nijmegen, **1992**.
[34] *TeXsan: Crystal Structure Analysis Package*, Molecular Structure Corporation, The Woodland, Texas (USA), **1985** and **1992**.
[35] SIR-97 in A. Altomare, M. C. Burla, M. Camalli, G. Cascarano, C. Giacovazzo, A. Guagliardi, A. G. G. Moliterni, G. Polidori, R. Spagna, *J. Appl. Crystallogr.* **1998**, *32*, 115.
[36] G. M. Sheldrick, SHELX97, Programs for Crystal Structure Analysis (Release 97–2), University of Göttingen, Germany, **1997**.
[37] A. P. Altshuller, I. R. Cohen, *Anal. Chem.* **1960**, *32*, 802–810.

Received: July 10, 2003 [F5322]